

Article

Path-Following and Obstacle-Avoidance Control of USV Based on Finite-Distance Convergence

Junbao Wei, Jianqiang Zhang *, Zhong Liu, Jianjing Qu , Bowen Sui and Yuanyuan Zhang

College of Weaponry Engineering, Naval University of Engineering, Wuhan 430030, China

* Correspondence: d22182601@nue.edu.cn

Abstract: The control problem of avoidance-path-following is a critical consideration in the research of unmanned surface vehicle (USV) navigation control, and it holds great significance for the navigation safety of USVs. A guidance and control scheme based on finite-distance convergence is proposed in this paper. First, the requirements for the USV to avoid obstacles from the perspective of path-following lateral error are analyzed. Then, a new performance function with finite-distance convergence is proposed to constrain the lateral error. Based on this, a heading guidance law and a backstepping controller are designed to ensure that the lateral error converges to a steady-state value within the prescribed navigation distance and that the stability is maintained, satisfying the requirements of obstacle avoidance for the USV. In addition, an adaptive velocity command is designed to adjust the velocity with the lateral error, which, to a certain extent, avoids the saturation of the heading actuator caused by the large lateral error. Finally, it is proven through theory and simulation that the control algorithm can guide the USV to achieve avoidance-path-following within a limited distance and to avoid obstacles effectively.

Keywords: USV; path-following and obstacle avoidance; guidance and control; finite-distance convergence; adaptive velocity command



Citation: Wei, J.; Zhang, J.; Liu, Z.; Qu, J.; Sui, B.; Zhang, Y. Path-Following and Obstacle-Avoidance Control of USV Based on Finite-Distance Convergence. *J. Mar. Sci. Eng.* **2024**, *12*, 34. <https://doi.org/10.3390/jmse12010034>

Academic Editor: Rafael Morales

Received: 9 November 2023

Revised: 14 December 2023

Accepted: 18 December 2023

Published: 22 December 2023



Copyright: © 2023 by the authors. Licensee MDPI, Basel, Switzerland. This article is an open access article distributed under the terms and conditions of the Creative Commons Attribution (CC BY) license (<https://creativecommons.org/licenses/by/4.0/>).

1. Introduction

Unmanned surface vehicles (USVs), as a type of small intelligent task platform, have developed rapidly in recent years due to their broad application prospects in marine scientific research, rescue and disaster response, and maritime security. Among the key technologies of USVs, navigation control technology has also attracted attention and research from numerous scholars.

USVs without a lateral thruster are a typical class of underactuated systems where the number of control inputs is fewer than the degrees of freedom that need to be controlled. Therefore, the navigation control technology for USVs presents certain challenges [1]. The line-of-sight (LOS) guidance method was first proposed in [2]. The heading command was designed based on the position of the USV and desired waypoints along the trajectory in this method, and the control variables of the USV were transformed from position and heading into heading and velocity to achieve path-following. Moreover, considering that traditional LOS guidance laws are susceptible to environmental interference, the authors of [3,4] proposed an integral LOS guidance law. To ensure that the USV maintains the stable tracking of a straight path, an integral term was used to compensate for the influence of ocean currents [3,4]. Considering that the LOS guidance method is difficult to apply to curved paths, this algorithm was not adopted in [5], whereas a controller was designed based on defining the lateral error between the USV and the curved path. The authors of [6] investigated the control problem of a USV tracking a piecewise linear path. Straight-line path-following was achieved by defining virtual target points along the desired path and designing corresponding algorithms for both their motion and that of the USV. Owing to the influence of environmental factors, such as wind, waves, and currents, disturbance

observers [7,8] and neural networks [9,10] have been used to improve the anti-interference performance of the control system in most studies. Additionally, the authors of [11–13] further considered input-saturation issues. In [12], an output redefinition control method was proposed, which relaxes the restrictions on the known and fixed saturation amplitude.

To improve the performance of USV path-following, finite-time convergence theories were introduced into the controller design [14–16]. In [16], a timed LOS guidance law and a timed heading controller were proposed to ensure that the tracking error converged in a fixed time, and the upper bound of the convergence time was determined by selecting specific parameters. Furthermore, prescribed performance was used to constrain tracking errors to ensure that the USV could achieve path-following within a predetermined time [17]. Additionally, with the emergence of artificial intelligence algorithms, such as reinforcement learning, these algorithms were applied to USV navigation control [18,19]. A reinforcement-learning-based path-following strategy was proposed in [19]. The path-following problem was decomposed into multiple tasks, and rewards were assigned to enhance the training efficiency and effectiveness of this strategy. However, owing to the relatively limited training environment, significant tracking errors may occur when a USV attempts to track paths in real-world environments.

In practice, the obstacle-avoidance problem of USVs in path-following control is very important for their navigation safety. Path planning for obstacle avoidance and the tracking control problem were combined [20–22]. The authors of [20] proposed a finite-time convergence path-following control scheme for a USV and further supplemented it with an obstacle-avoidance strategy. The obstacle-avoidance strategy was proposed to plan the path according to the real-time movement of obstacles and the degree of danger [22]. However, the above studies did not consider the influence of the path-following error on obstacle avoidance in the tracking control process. Even if the pre-planned path could avoid obstacles, deviation from the path still resulted in collisions between the USV and obstacles. To solve this problem, path-following and obstacle-avoidance control schemes were proposed based on a model predictive control method [23,24]. Constraints were designed in [23], such as maintaining a minimum distance between the USV and obstacles and limiting the actuator's output to allow the USV to avoid obstacles and follow the path. The authors of [24] proposed a model predictive control strategy by incorporating an auxiliary trajectory. However, the model predictive control method encountered difficulties in setting the prediction step size and involved extensive computational requirements, which limits its practical applicability.

To address the control problem of path-following and obstacle avoidance for the USV, a two-step design strategy is proposed in this paper: (1) The USV used in this study realizes the tracking of the avoidance path within the prescribed navigation distance. It ensures that no collision occurs by setting this distance to be shorter than the distance between the USV and the obstacle. (2) The USV maintains a stable tracking of the avoidance path. The path deviation error is limited to the specified convergence range, ensuring that the USV consistently maintains a safe distance from the obstacle. The contributions of this paper are as follows:

1. The prescribed performance method was used to improve the transient and steady-state performance of the USV's control system. The tracking error was limited to a steady-state value within a prescribed navigation distance. As the adjustable parameters, the convergence distance and steady-state value are straightforward to set, making the method convenient for practical application in various scenarios.
2. Considering the USV is in sea areas with obstacles, a guidance and control strategy was proposed for avoidance path-following. The USV could achieve path-following and obstacle avoidance, ensuring stable path-following while maintaining a safe distance from obstacles.
3. The designed adaptive velocity command could be adjusted based on the magnitude of the lateral error. When the USV deviates from the desired path, the velocity value is automatically reduced. In conjunction with a predetermined convergence distance,

the corresponding increase in convergence time greatly helps to mitigate saturation issues in the heading actuator.

The remainder of this paper is organized as follows: Section 2 discusses the preliminaries; Sections 3 and 4 present the guidance and control law design process; Sections 5 and 6 provide a stability analysis and simulation study, respectively; and Section 7 presents the conclusions.

2. Preliminaries

2.1. USV Model

For the path-following problem of the USV, the following three-degree-of-freedom kinematics and dynamics models are usually established and studied [25]:

$$\begin{cases} \dot{\boldsymbol{\eta}} = \mathbf{J}(\boldsymbol{\psi})\boldsymbol{v} \\ \dot{\boldsymbol{v}} = \mathbf{M}^{-1}(\mathbf{F}(\boldsymbol{v}) - \mathbf{C}\boldsymbol{v} + \boldsymbol{\tau}) + \mathbf{D} \end{cases} \quad (1)$$

with

$$\mathbf{J}(\boldsymbol{\psi}) = \begin{bmatrix} \cos \psi & -\sin \psi & 0 \\ \sin \psi & \cos \psi & 0 \\ 0 & 0 & 1 \end{bmatrix}, \quad (2)$$

where $\boldsymbol{\eta} = [x, y, \psi]^T$, x and y are the position of the vehicle in inertial coordinates. ψ represents the heading angle. $\boldsymbol{v} = [u, v, r]^T$, u and v stand for the vessel surge and sway velocity, respectively. r represents the yaw angular velocity. $\boldsymbol{\tau} = [\tau_u, 0, \tau_r]^T$, τ_u and τ_r denote the surge force and the yaw moment, respectively, as the control inputs. $\mathbf{M} = \text{diag}(m_{11}, m_{22}, m_{33})$ represents the inertia coefficient matrix, $\mathbf{F}(\boldsymbol{v}) = [m_{22}vr, -m_{11}ur, (m_{11} - m_{22})uv]^T$, and $\mathbf{C} = \text{diag}(d_{11}, d_{22}, d_{33})$ represents the hydrodynamic damping matrix. $\mathbf{D} = [d_u, d_v, d_r]^T$ stands for external disturbances, and the following assumption is made [26]:

Assumption 1. *The disturbance terms d_i ($i = u, v, r$) and their first derivatives are bounded.*

2.2. Analysis of USV Path-Tracking and Obstacle Avoidance

As shown in Figure 1, the USV is in the sea area with obstacles, and the avoidance path is connected by waypoints P_1, P_2, P_3 . OXY represents the geodetic coordinate system while SX_bY_b represents the body coordinate system of the USV [12,27]. According to the appearance parameters of the USV, the obstacle is set to a safe boundary of a certain radius, and the USV can be regarded as a particle for subsequent analysis. R_2 represents the update radius of the waypoint, i.e., when the USV enters the range, it changes from line segment P_1P_2 to line segment P_2P_3 tracking [28]. The lateral error e_d represents the distance from the USV to the desired path. ψ_1, ψ_2 represent the azimuth of each path, respectively.

d_A, d_C represent the distance between the obstacle A, C and the USV, respectively, d_B, d_D represent the distance between the obstacle B, D and the desired path, respectively. To measure d_C in advance, it can be approximated as $d_{C1} = R_2 + d_{CP2}$. For the convenience of explanation, d_1 is used to represent the distance between the USV and the obstacle and d_2 represents the distance between the path and the obstacle.

Remark 1. *In this paper, the security threats posed by obstacles in the area are categorized into two distinct types: (1) Obstacles positioned ahead of the navigation direction of the USV require the USV to track an avoidance path to steer clear of them, such as obstacles A, C ; (2) Obstacles located on either side of the intended path require the USV to maintain stable path-tracking to evade potential collisions, such as obstacles B, D . To ensure effective obstacle avoidance during navigation, the USV must consistently track the obstacle-avoidance path within the designated navigation distance d_1 . In the subsequent tracking process, the lateral error e_d satisfies $|e_d| < d_2$.*

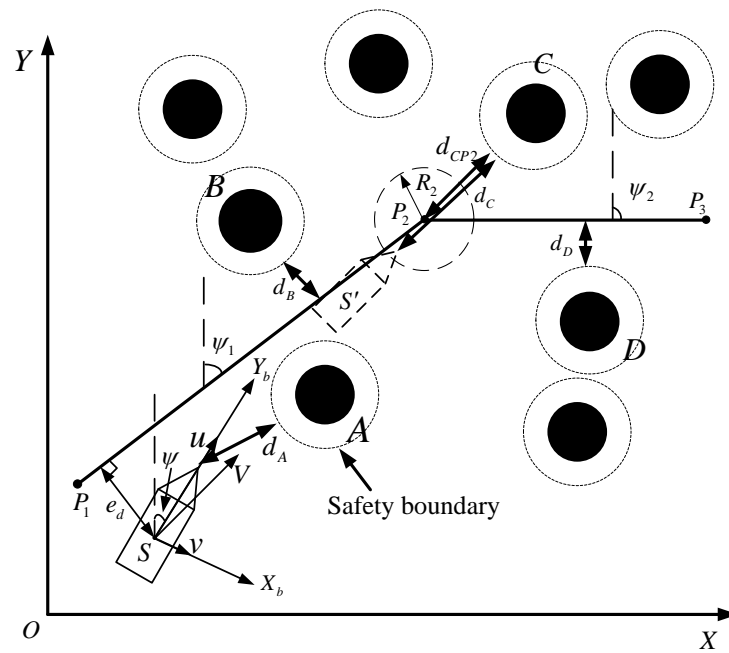


Figure 1. Schematic diagram of USV tracking path and obstacle avoidance.

According to Figure 1, the following differential equation of lateral error can be established:

$$\dot{e}_d = u \sin(\psi - \alpha) + v \cos(\psi - \alpha). \tag{3}$$

Noting that $\beta = \arctan(\frac{v}{u})$, the resultant velocity is $V = \sqrt{u^2 + v^2}$, Equation (3) is reduced to

$$\dot{e}_d = V \sin(\psi - \alpha - \beta). \tag{4}$$

The purpose of this paper is to propose a guidance and control strategy with finite-distance convergence that facilitates the lateral error e_d to converge to a steady-state value within a predetermined navigation distance and to keep it within a limited range. In essence, the USV accomplishes the tracking of the obstacle-avoiding path before reaching a navigation distance value of d_1 and then sustains a deviation error smaller than d_2 at a certain distance from the obstacle during subsequent tracking. Finally, the path-tracking and obstacle avoidance of the USV are realized to ensure the safety of navigation. The guidance and control framework of the USV is shown in Figure 2.

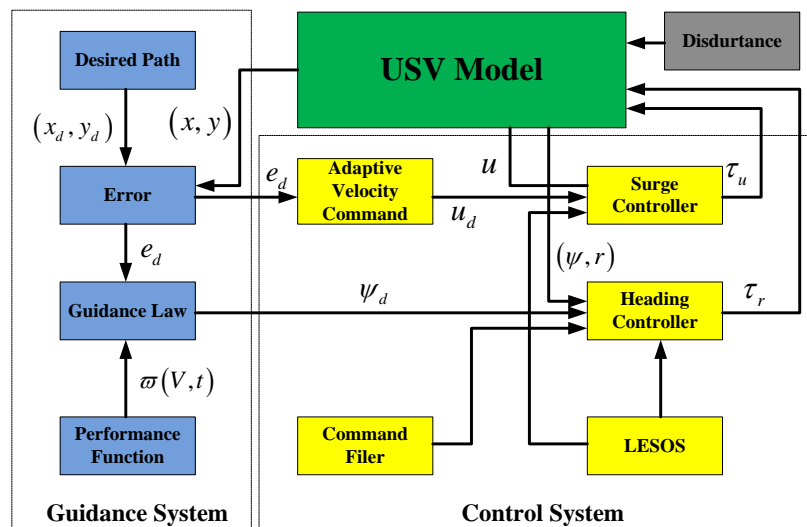


Figure 2. Frame diagram of guidance and control scheme.

2.3. Command Filter

The command filter designed in [29] is shown below:

$$\begin{cases} \dot{\chi}_1 = \chi_2 \\ \dot{\chi}_2 = 2\zeta\omega \left(\frac{\omega^2}{2\zeta\omega} (x_d - \chi_1) - \chi_2 \right) \end{cases}, \quad (5)$$

where x_d is the input of the filter, and the output χ_1 and χ_2 are the estimated values of x_d and its first derivative \dot{x}_d , respectively. ζ, ω are filter parameters and $\zeta \in (0, 1], \omega > 0$.

According to the convergence conclusion of the filter in [29]: $\lim_{\omega \rightarrow \infty} \chi_1 = x_d, \lim_{\omega \rightarrow \infty} \chi_2 = \dot{x}_d$, the following assumption can be made:

Assumption 2. There are unknown constants $\eta_1, \eta_2 > 0$ such that $|\chi_1 - x_d| \leq \eta_1$ and $|\chi_2 - \dot{x}_d| \leq \eta_2$.

2.4. Nonlinear Disturbance Observer (NDO)

Considering the following first-order uncertain system:

$$\begin{cases} \dot{x}_1(t) = f(x_1) + g(x_1)u + d(t) \\ y = x_1(t) \end{cases}, \quad (6)$$

where $d(t)$ represents the uncertain term, it is assumed that $d(t)$ is continuous, and its first derivative is bounded.

To estimate the unknown disturbance $d(t)$, the following NDO is designed with reference to [30]:

$$\begin{cases} \dot{\hat{x}}_1 = f(x_1) + g(x_1)u + \hat{x}_2 \\ \dot{\hat{x}}_2 = -K^2 \left(l_1 \arctan(\hat{x}_1 - x_1) + l_2 \arctan\left(\frac{\hat{x}_2}{K}\right) \right) \end{cases} \quad (7)$$

where \hat{x}_1 is the estimation value of x_1 . \hat{x}_2 is the estimation value of $d(t)$. $K > 0, l_i > 0 (i = 1, 2)$.

According to [30] on the proof of NDO convergence that the observation error $\tilde{d} = \hat{x}_2 - d$ is bounded, the assumption can be made as follows:

Assumption 3. NDO estimation error \tilde{d} is bounded, and there exists an unknown constant $\tilde{D} > 0$, such that $|\tilde{d}| \leq \tilde{D}$.

3. Guidance Law Design

3.1. Design of Finite-Distance Convergence Performance Function

The prescribed performance [31] method includes a performance function and error transformation, which means that while the tracking error converges in an arbitrarily small set, the convergence rate and overshoot of the tracking error satisfy the prescribed conditions.

The conventional performance function is expressed as follows:

$$\omega(t) = (\omega_0 - \omega_\infty) \exp(-\mu t) + \omega_\infty, \quad (8)$$

where $\omega_0, \mu, \omega_\infty$ are constants and $\omega_0 > \omega_\infty > 0, \mu > 0$. ω_∞ is the steady-state value and $\lim_{t \rightarrow \infty} \omega(t) = \omega_\infty$.

The performance function is positive and is continuously bounded and monotonically decreasing. The constraint of the function on the system tracking error $e(t)$ satisfies

$$-\omega(t) < e(t) < \omega(t). \quad (9)$$

The traditional performance function could force the tracking error to converge to the steady-state range in a finite time, enhancing the transient and steady-state performance of the control system. However, in scenarios where the presence of an obstacle at a distance d_1 in front of the USV's navigation direction is known, a finite-time convergence controller

may not ensure that the USV can avoid the obstacle and track the avoidance path before reaching a distance d_1 . Therefore, it is essential to propose a finite-distance convergence method to address this issue, specifically to achieve avoidance path-following within the constrained navigation distance of the USV and ensure the safety of its navigation.

Based on the above analysis, a new performance function with finite-distance convergence is proposed in this paper, as shown below:

$$\omega(V_0, t) = \begin{cases} \frac{\omega_0 - \omega_\infty}{R_0^2} \left(\int_{t_0}^t V_0 dt - R_0 \right)^2 \exp(-\mu t) + \omega_\infty, \int_{t_0}^t V_0 dt \leq R_0 \\ \omega_\infty, \int_{t_0}^t V_0 dt > R_0 \end{cases}, \quad (10)$$

where V_0 is velocity. $R_0 > 0$ is the set convergence distance for $\omega(t)$ converging to the steady-state value ω_∞ . t_0 is the initial time and $t \geq t_0$. The designed performance function converges to the steady-state value ω_∞ at $\int_{t_0}^t V_0 dt = R_0$, which is a positively continuous, bounded, and monotone decreasing function.

Remark 2. According to Remark 1, when the specific value of d_1 and d_2 are known, the parameter values of the convergence distance R_0 and the steady-state value ω_∞ of the performance function can be set, such that $R_0 \leq d_1$ and $\omega_\infty \leq d_2$. The designed function ensures that the lateral error between the USV and the avoidance path converges to the steady-state value within a limited navigation distance and remains stable, i.e., the USV will not collide with the obstacle and realize the tracking of the avoidance path before the navigation distance reaches R_0 . Subsequently, it will maintain a certain safe distance from the obstacle during stable tracking.

Because it is difficult to design the controller directly using inequality (9), it is necessary to convert the inequality constraints into equality constraints, as follows:

$$e(t) = \omega(t)S(\phi), \quad (11)$$

where ϕ is the transformation error, $S(\phi) = \frac{e^\phi - e^{-\phi}}{e^\phi + e^{-\phi}}$ is the transformation function. It can be easily observed that $S(\phi)$ is a smooth and strictly increasing reversible function.

Furthermore, the inverse transformation of $S(\phi)$ is performed as follows:

$$\phi = S^{-1}(e, \omega) = \frac{1}{2} \ln \left(\frac{1 + e/\omega}{1 - e/\omega} \right). \quad (12)$$

Remark 3. If $\phi(t) \in l_\infty$ can be satisfied under the condition of $\forall t \in [0, \infty)$, where $-1 < S(\phi) < 1$, then inequality (9) holds. In addition, the system tracking error is limited to within the prescribed range. Based on the properties of the designed performance function, the tracking error converges to a steady-state value in a finite time and satisfies the prescribed transient and steady-state performance requirements.

3.2. Guidance Law Design

For the lateral error e_d in Equation (4), the following finite-time convergence performance function is designed:

$$\omega(V, t) = \begin{cases} \frac{\omega_0 - \omega_\infty}{R^2} \left(\int_{t_0}^t V dt - R \right)^2 \exp(-\mu t) + \omega_\infty, \int_{t_0}^t V dt \leq R \\ \omega_\infty, \int_{t_0}^t V dt > R \end{cases}, \quad (13)$$

where $\omega_0, \omega_\infty, \sigma$ are performance function parameters, t_0 is the initial time and $t \geq t_0$. $R > 0$ are the prescribed convergence distance, and u is the velocity of the USV.

According to Equation (12), the position deviation is transformed to obtain the following transformation error ε :

$$\varepsilon = \frac{1}{2} \ln \left(\frac{1 + e_d/\omega}{1 - e_d/\omega} \right). \tag{14}$$

Combining of Equation (4), the derivation of Equation (14) can be obtained

$$\dot{\varepsilon} = \varphi_1 (\dot{e}_d - e_d \varphi_2), \tag{15}$$

where $\varphi_1 = \frac{1}{1-(e/\omega)^2} \cdot \frac{1}{\omega} > 0$, $\varphi_2 = \frac{\dot{\omega}}{\omega^2}$.

The following Lyapunov function is established for the transformation error ε :

$$W_1 = \frac{1}{2} \varepsilon^2. \tag{16}$$

Combining of Equation (15), the derivation of Equation (16) can be obtained as follows:

$$\dot{W}_1 = \varepsilon \left(\varphi_1 \left(\sqrt{u^2 + v^2} \sin(\psi - \alpha + \beta) \right) - e_d \varphi_2 \right). \tag{17}$$

The heading guidance law is designed as follows:

$$\psi_d = \alpha - \beta + \arcsin \left(\frac{-k_\psi \varepsilon + e_d \varphi_2}{\varphi_1 \sqrt{u^2 + v^2}} \right), \tag{18}$$

where $k_\psi > 0$ is the parameter to be designed.

Substitute Equation (18) into Equation (17), we obtain

$$\dot{W}_1 = \varepsilon \left(-\cos(\psi - \psi_d) k_\psi \varepsilon + \varphi_1 \sqrt{u^2 + v^2} \sin(\psi - \psi_d) \cos \left(\arcsin \left(\frac{-k_\psi \varepsilon + e_d \varphi_2}{\varphi_1 \sqrt{u^2 + v^2}} \right) \right) \right). \tag{19}$$

Similar to [32], when $\psi \rightarrow \psi_d$, it is obviously easy to obtain

$$\dot{W}_1 = -k_\psi \varepsilon^2 < 0. \tag{20}$$

Remark 4. According to Equation (4), ε is bounded when $\psi \rightarrow \psi_d$. Furthermore, according to Remark 3, the lateral error e_d satisfies the constraint requirements of the performance function and converges to the steady-state value within a limited distance, i.e., the USV realizes the tracking of the avoidance path within a prescribed limited distance.

4. Controller Design

Control objective: Considering the presence of obstacles in the sea area, the heading control law for the USV is designed based on the heading guidance law, and the USV could track the avoidance path within a limited navigation distance to avoid collision with obstacles. Subsequently, the velocity of the USV is adaptively regulated to mitigate the potential saturation of the heading actuator when the USV approaches the turning point of the straight path.

For the motion model of USV, this section is divided into two parts to design the heading and velocity control laws, respectively, to realize the avoidance path-following of USV.

4.1. Design of Heading Control Law

The heading error e_ψ is defined as follows:

$$e_\psi = \psi - \psi_d. \tag{21}$$

Combining of Equation (1), the derivation of Equation (21) can be obtained

$$\dot{e}_\psi = r - \dot{\psi}_d. \tag{22}$$

Since it is difficult to accurately obtain the first derivative of ψ_d , the following command filter is designed to estimate $\dot{\psi}_d$:

$$\begin{cases} \dot{\chi}_{\psi 1} = \chi_{\psi 2} \\ \dot{\chi}_{\psi 2} = 2\zeta_\psi \omega_\psi \left(\frac{\omega_\psi^2}{2\zeta_\psi \omega_\psi} (\psi_d - \chi_{\psi 1}) - \chi_{\psi 2} \right) \end{cases}, \tag{23}$$

where $\chi_{\psi 1}$ and $\chi_{\psi 2}$ are the estimated values of ψ_d and its first derivative $\dot{\psi}_d$, respectively. $0 < \zeta_\psi < 1$ and $\omega_\psi > 0$ are the parameters to be designed.

The Lyapunov function is defined as follows:

$$W_2 = \frac{1}{2} e_\psi^2. \tag{24}$$

Combining Equation (22) and differentiating Equation (24), we obtain

$$\dot{W}_2 = e_\psi (r - \chi_{\psi 2} + \eta_\psi), \tag{25}$$

where $\eta_\psi = \dot{\psi}_d - \chi_{\psi 2}$ is the filter error.

The control law of the heading angular velocity r is designed:

$$r_d = -k_\psi e_\psi + \chi_{\psi 2}, \tag{26}$$

where $k_\psi > 0$ is the parameter to be designed.

The heading angular velocity error e_r is defined as follows:

$$e_r = r - r_d. \tag{27}$$

Combining Equation (1), the derivation of Equation (27) can be obtained

$$\dot{e}_r = f_r + g_r \tau_r + d_r - \dot{r}_d, \tag{28}$$

where $f_r = \frac{1}{m_{33}}((m_{11} - m_{22})uv - d_{33}r)$, $g_r = \frac{1}{m_{33}}$.

The Lyapunov function is defined as follows:

$$W_3 = \frac{1}{2} e_r^2. \tag{29}$$

Combining Equation (28) and differentiating Equation (29), we obtain

$$\dot{W}_3 = e_r (f_r + g_r \tau_r + d_r - \dot{r}_d). \tag{30}$$

The guidance law of the heading subsystem is designed:

$$\tau_r = \frac{1}{g_r} \left(-k_r e_r - e_\psi - f_r - \hat{d}_r + \chi_{r2} \right), \tag{31}$$

where $k_r > 0$ is the parameter to be designed. \hat{d} is the NDO estimate of the external disturbance d_r . χ_{r2} represents the estimated derivative of the virtual control law, which could be acquired through the following command filter:

$$\begin{cases} \dot{\chi}_{r1} = \chi_{r2} \\ \dot{\chi}_{r2} = 2\zeta_r \omega_r \left(\frac{\omega_r^2}{2\zeta_r \omega_r} (r_d - \chi_{r1}) - \chi_{r2} \right) \end{cases}, \tag{32}$$

where $0 < \zeta_r < 1$ and $\omega_r > 0$ are the parameters to be designed.

4.2. Design of Velocity Control Law

Considering most of the literature in the study of path-following, the velocity of the USV is typically maintained at a constant value. However, as the USV approaches the turning point of the straight path, this constant velocity results in a larger turning radius, requiring increased output from the heading actuator and making it susceptible to saturation.

In response to this issue, an adaptive velocity command is proposed as follows:

$$u_d = u_0 - \lambda \frac{2}{\pi} \arctan\left(e_d^2\right), \tag{33}$$

where $u_0 > 0$ is a constant velocity value. $\lambda > 0$ is the parameter to be designed and $\lambda < u$.

Remark 5. Diverging from the majority of the existing literature, the designed velocity command can be adaptively adjusted based on the error size, offering the following three advantages: (1) When encountering a significant tracking error, the command could reduce the velocity of the USV, subsequently minimizing the turning radius and largely preventing saturation of the heading actuator. (2) The velocity's variation with the command minimally impacts the finite-distance convergence performance of the tracking error, ensuring the USV's ability to follow the avoidance path effectively. (3) The designed velocity command value consistently remains above 0, aligning with practical requirements.

The following velocity tracking error e_u is defined:

$$e_u = u - u_d. \tag{34}$$

On differentiating Equation (34) combining Equations (1) and (4), we obtain

$$\dot{e}_u = f_u + g_u \tau_u + d_u - \dot{u}_d, \tag{35}$$

where $f_u = \frac{1}{m_{11}}(m_{22}vr - d_{11}u)$, $g_u = \frac{1}{m_{11}}$, $\dot{u}_d = -\frac{4\lambda e_d \dot{e}_d}{\pi(1+e_d^4)}$.

The Lyapunov function is defined as follows:

$$W_3 = \frac{1}{2} e_u^2. \tag{36}$$

On differentiating Equation (36) combining Equation (35), we obtain

$$\dot{W}_3 = e_u (f_u + g_u \tau_u + d_u - \dot{u}_d). \tag{37}$$

The control law of the velocity subsystem is designed as follows:

$$\tau_u = \frac{1}{g_u} \left(-k_u e_u - f_u - g_u - \hat{d}_u + \dot{u}_d \right), \tag{38}$$

where $k_r > 0$ is the parameter to be designed. \hat{d} is the NDO estimate of external disturbance d_r .

5. Stability Analysis

Theorem 1. For the USV model (1) and the lateral error model (4), under assumptions 1, 2, and 3, the heading guidance law (18) and the system control laws (31) and (38) are applied to the USV control system based on the designed performance function (10), the following conclusions are obtained:

1. The errors e_ψ, e_r, e_u of the USV control system are bounded, and the lateral error e_d converges to the steady-state value within a finite distance.
2. The USV realizes the tracking of the avoidance path within the prescribed distance R and avoids colliding with obstacles. When the navigation distance exceeds R , the USV maintains stable path-tracking and keeps a safe distance from obstacles.

Proof of Theorem 1. The following Lyapunov function is defined:

$$W = \frac{1}{2} (e_\psi^2 + e_r^2 + e_u^2). \tag{39}$$

On differentiating Equation (39) combining Equations (25), (30) and (37), we obtain

$$\dot{W} = e_\psi (r - \chi_{\psi 2} + \eta_\psi) + e_r (f_r + g_r \tau_r + d_r - \dot{r}_d) + e_u (f_u + g_u \tau_u + d_u - \dot{u}_d). \tag{40}$$

Substituting Equations (26), (31) and (38) into Equation (40), we obtain

$$\dot{W} = -k_\psi e_\psi^2 + e_\psi (\chi_{\psi 2} - \dot{\psi}_d) - k_r e_r^2 + e_r (\chi_{r 2} - \dot{r}_d + (-\hat{d}_r + d_r)) - k_u e_u^2 + e_u (-\hat{d}_u + d_u). \tag{41}$$

According to Assumptions 1, 2, and 3, there are different bounded constants $N_i (i = 1, 2, 3, 4) > 0$ such that in Equation (41), there is

$$\begin{cases} |\chi_{\psi 2} - \dot{\psi}_d| \leq N_1 \\ |\chi_{r 2} - \dot{r}_d| \leq N_2 \\ |-\hat{d}_r + d_r| \leq N_3 \\ |-\hat{d}_u + d_u| \leq N_4 \end{cases}. \tag{42}$$

According to Young’s inequality, there is

$$\begin{cases} e_\psi (\chi_{\psi 2} - \dot{\psi}_d) \leq \frac{k_\psi}{2} e_\psi^2 + \frac{1}{2k_\psi} N_1^2 \\ e_r (\chi_{r 2} - \dot{r}_d) \leq \frac{k_r}{4} e_r^2 + \frac{1}{k_r} N_2^2 \\ e_r (-\hat{d}_r + d_r) \leq \frac{k_r}{4} e_r^2 + \frac{1}{k_r} N_3^2 \\ e_u (-\hat{d}_u + d_u) \leq \frac{k_u}{2} e_u^2 + \frac{1}{2k_u} N_4^2 \end{cases}. \tag{43}$$

Furthermore, Equation (41) can be reduced to

$$\dot{W} \leq -\frac{k_\psi}{2} e_\psi^2 - \frac{k_r}{2} e_r^2 - \frac{k_u}{2} e_u^2 + \frac{1}{2k_\psi} N_1^2 + \frac{1}{k_r} (N_2^2 + N_3^2) + \frac{1}{2k_u} N_4^2. \tag{44}$$

Let $\bar{k} = \min\{k_r, k_\psi, k_u\}$, $M = \max\{N_1^2, N_2^2, N_3^2, N_4^2\}$. Then, the following can be further obtained

$$\dot{W} \leq -\bar{k}W + \left(\frac{1}{2k_\psi} + \frac{1}{k_r} + \frac{1}{2k_u} \right) M. \tag{45}$$

When $W > \frac{\left(\frac{1}{2k_\psi} + \frac{1}{k_r} + \frac{1}{2k_u} \right) M}{\bar{k}}$, it is obvious that $\dot{W} < 0$, indicating that W is bounded. According to the definition W , it can be obtained that e_ψ, e_r, e_u is bounded. According to Remark 3, e_d satisfies the following inequality.

$$-\omega(u, t) < e_d < \omega(u, t). \tag{46}$$

Because the performance function converges to the steady-state value ω_∞ at the navigation distance $\int_{t_0}^t V dt = R$, e_d is bounded and converges to the steady-state value within the prescribed distance R .

By setting the convergence distance parameter R to ensure $R < d_1$ and referencing the conclusion of 1, the USV achieves the tracking of the avoidance path within the distance R and does not collide with the obstacle.

When the navigation distance exceeds R , the performance function $\omega(V, t)$ satisfies $\omega \in (-\omega_\infty, \omega_\infty)$, and then $e_d \in (-\omega_\infty, \omega_\infty)$. By setting the steady-state value ω_∞ to ensure $\omega_\infty < d_2$, the USV could achieve stable tracking of the avoidance path and maintain a certain safe distance from the obstacles. \square

6. Simulation Results

To verify the effectiveness of the guidance and control scheme, the USV model (1) and the lateral error model (4) were employed, and the guidance and control strategy proposed in Sections 3 and 4 was implemented for MATLAB simulation. The model parameters are presented in Table 1.

Table 1. Model parameters.

Parameters	Values	Parameters	Values
m_{11}	200 kg	d_{11}	70 kg/s
m_{22}	250 kg	d_{22}	100 kg/s
m_{33}	80 kg·m ²	d_{33}	50 (kg·m ²)/s

Based on Figure 1, the simulation scenario for tracking the path of the USV and avoiding obstacles is designed as depicted in Figure 3. The initial position of the USV is set to $[x, y]^T = [20 \text{ m}, 0]^T$, the initial heading angle is $\psi = 0.8\text{rad}$, and the initial values of other state variables is $[u, v, r]^T = [3 \text{ m/s}, 0.1 \text{ m/s}, 0]^T$. The obstacle-avoidance path consists of 5 waypoints $\{P_1(0, 0), P_2(50, 30), P_3(70, 50), P_4(100, 105), P_5(120, 180)\}$, and there are several obstacles near the USV's location. By measuring d_1, d_2 and referring to Remark 1, the convergence distance and the steady-state value can be set $R = 20 \text{ m}$, $\omega_\infty = 1 \text{ m}$ to ensure that $R < d_1$, $\omega_\infty < d_2$. The simulation parameter values are shown in Table 2.

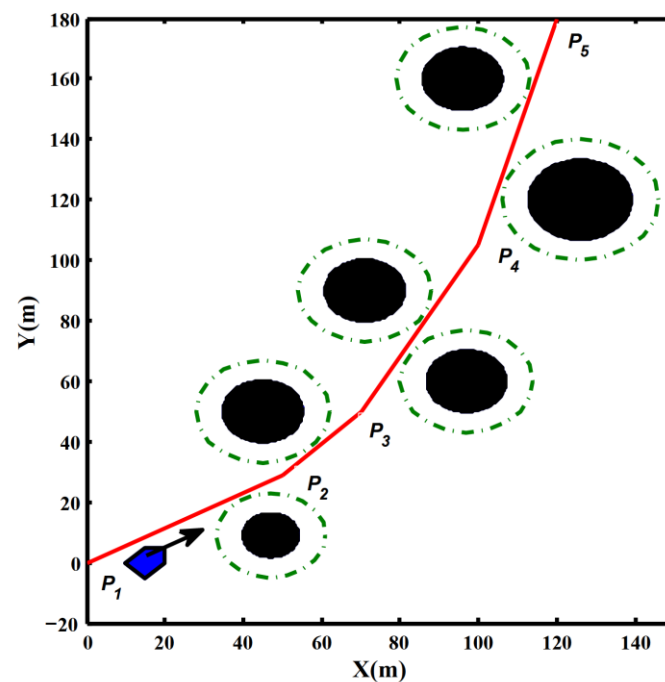


Figure 3. Simulation scenarios of USV tracking path and obstacle avoidance.

Table 2. Simulation parameters.

Parameters	Values	Parameters	Values	Parameters	Values
ω_0	30 m	k_e	0.2	λ	3
ω_∞	1 m	k_ψ	0.3	ζ_ψ	0.5
μ	0.2	k_r	0.5	ζ_r	0.5
R	20 m	k_u	0.5	ω_ψ	10
t_0	0	u_0	5 m/s	ω_r	5

6.1. Case 1

To demonstrate the superiority of the guidance and control scheme proposed in this paper (denoted as “A”), the control scheme based on ESHLOS guidance law proposed in [10] (denoted as “B”) is compared and simulated. The simulation results are shown in Figures 4–9.

As shown in Figure 4, Scheme A’s USV could adjust its heading within a limited distance to track the avoidance path without colliding with obstacles. It maintains stable path-following, with a small lateral error and a distance from the safe boundary of the obstacle. The scheme ensures the safe navigation of the USV. Although Scheme B could basically track the desired path, there is a certain deviation in its trajectory, which leads to entering the safe boundary of the obstacle. This scheme has the risk of collision with the obstacle. The main reason for the above results is that the lateral error of Scheme A is always constrained by the designed performance function, converges within a prescribed finite distance, and remains stable, which satisfies the requirements of obstacle avoidance (refer to Figure 5). The lateral error of Scheme B lacks specific constraints, resulting in slow convergence and a large steady-state value within the same distance, which leads to the risk of collision obstacles. In addition, it is noted that the waypoint update time differs between Scheme A and B. The adaptive velocity of Scheme A is adjusted based on the path-following error, resulting in an average velocity that is lower than Scheme B’s (refer to Figure 6). Although this factor affects the convergence time of the lateral error, greater emphasis is placed on the performance of finite-distance convergence in this paper, and obstacle avoidance is achieved through this method.

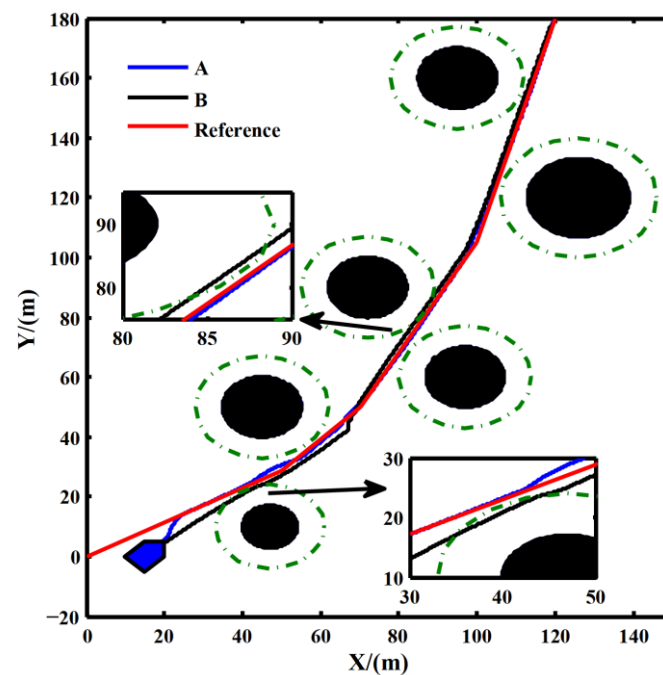


Figure 4. Path-tracking and obstacle avoidance of USV.

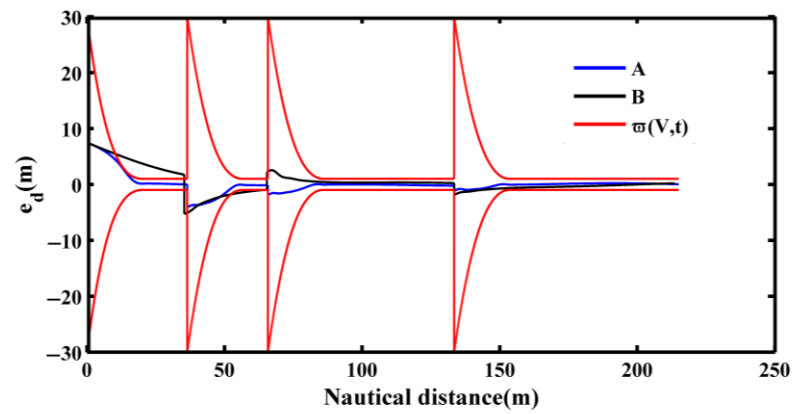


Figure 5. Curves of tracking error changing with navigation distance.

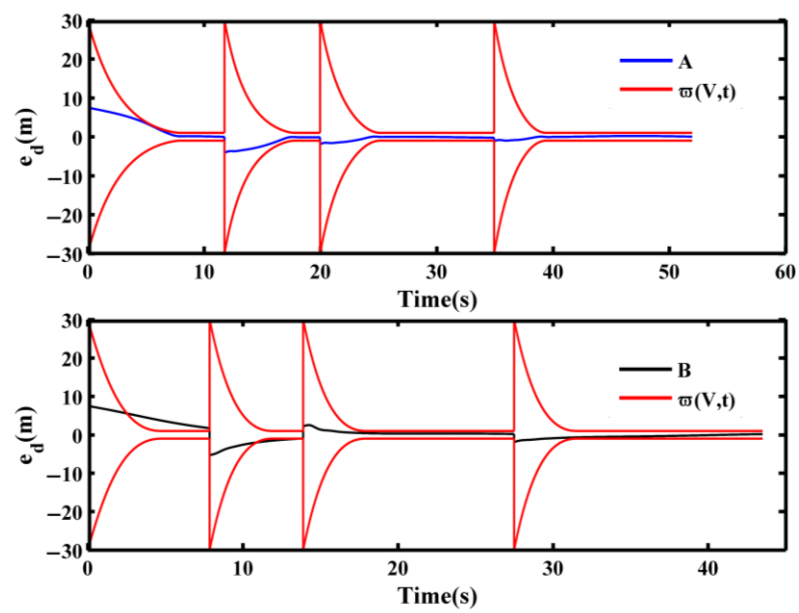


Figure 6. Curves of tracking error changing with time.

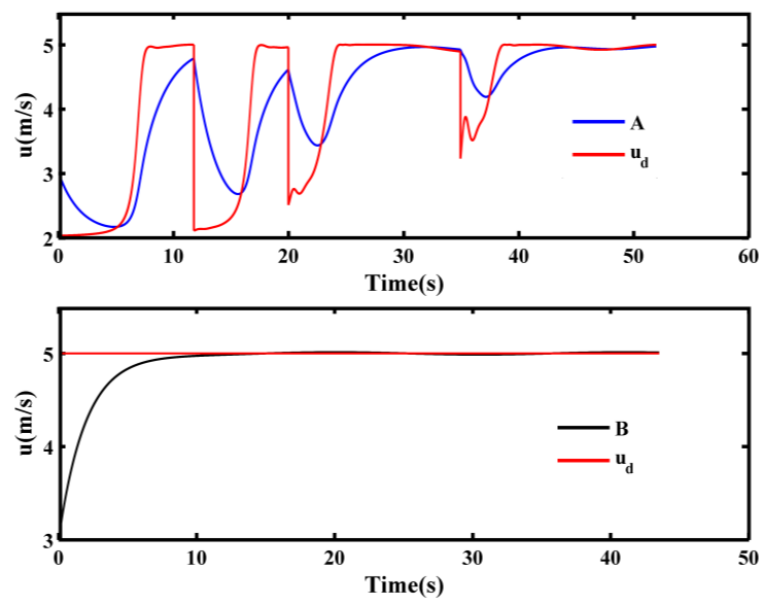


Figure 7. Curves of USV velocity tracking.

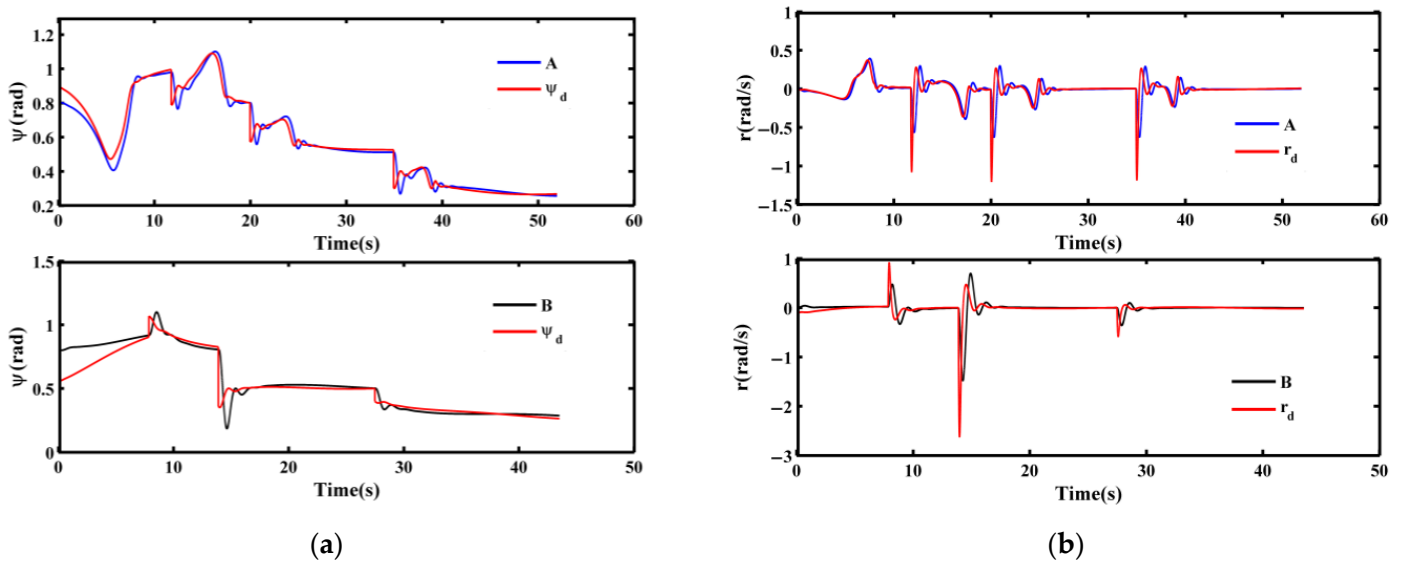


Figure 8. Curves of USV state variable tracking: (a) Curves of heading angle tracking; (b) Curves of heading angular velocity tracking.

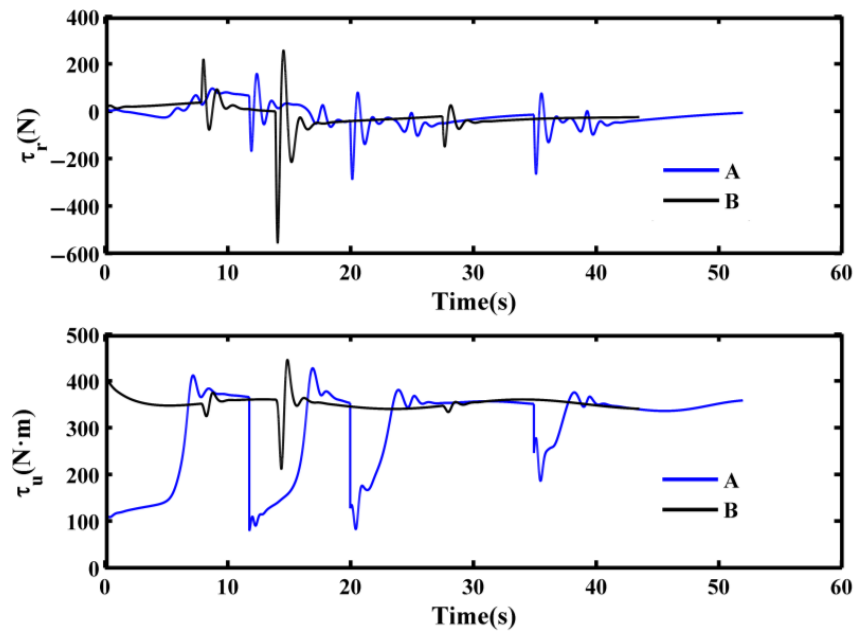


Figure 9. Curves of USV control input.

6.2. Case 2

To reflect the superiority of the adaptive velocity command. The guidance and control scheme proposed in this paper (denoted as “C”) is compared with the scheme without adaptive velocity command (denoted as “D”). The simulation results are shown in Figures 10–14.

As shown in Figure 10, both Schemes C and D could track the avoidance path. In addition, the lateral error converges to the steady-state value within a prescribed finite distance and remains stable, satisfying the requirements of avoiding obstacles. Figure 13 reveals that the velocity of Scheme D tends towards a constant value, while the velocity of Scheme C is adjusted based on the lateral error magnitude, which always remains above 0. It is evident from Figure 14 that as the USV transitions to the subsequent waypoint for tracking, the heading actuator τ_r exhibits some degree of fluctuation. It is apparent that the alteration in Scheme C is minimal, therefore mitigating the saturation of τ_r to some

extent. This is attributed to the velocity of Scheme C decreasing with the command (refer to Figure 13). At an equidistant convergence point (refer to Figure 11), the prolonged convergence time results in a lesser amplitude of change in the heading actuator τ_r . Additionally, the adjustment of the velocity command in Scheme C results in fluctuations in the amplitude of the velocity actuator τ_u , with its maximum value remaining comparable to that of Scheme D. In general, the implementation of an adaptive velocity command design could effectively mitigate the saturation of τ_r to a certain extent and has minimal impact on the finite-distance convergence performance of the lateral error, which ensures the path-following and obstacle-avoidance ability of the USV.

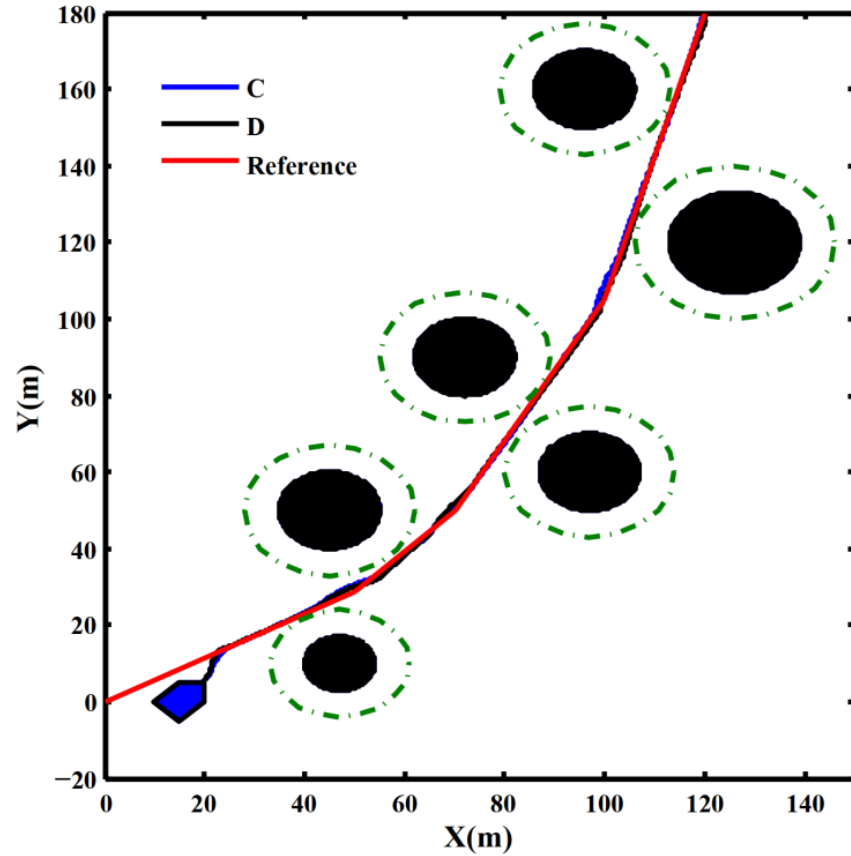


Figure 10. USV path-tracking and obstacle avoidance.

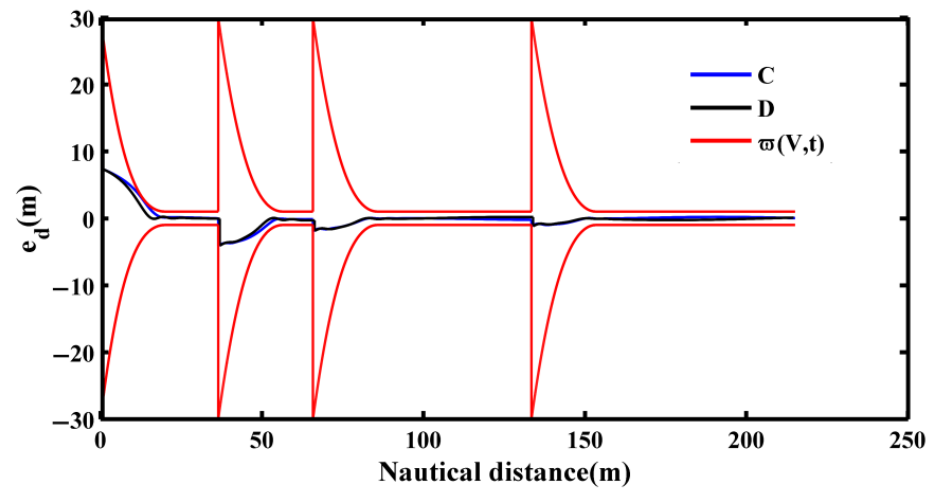


Figure 11. Curves of tracking error changing with navigation distance.

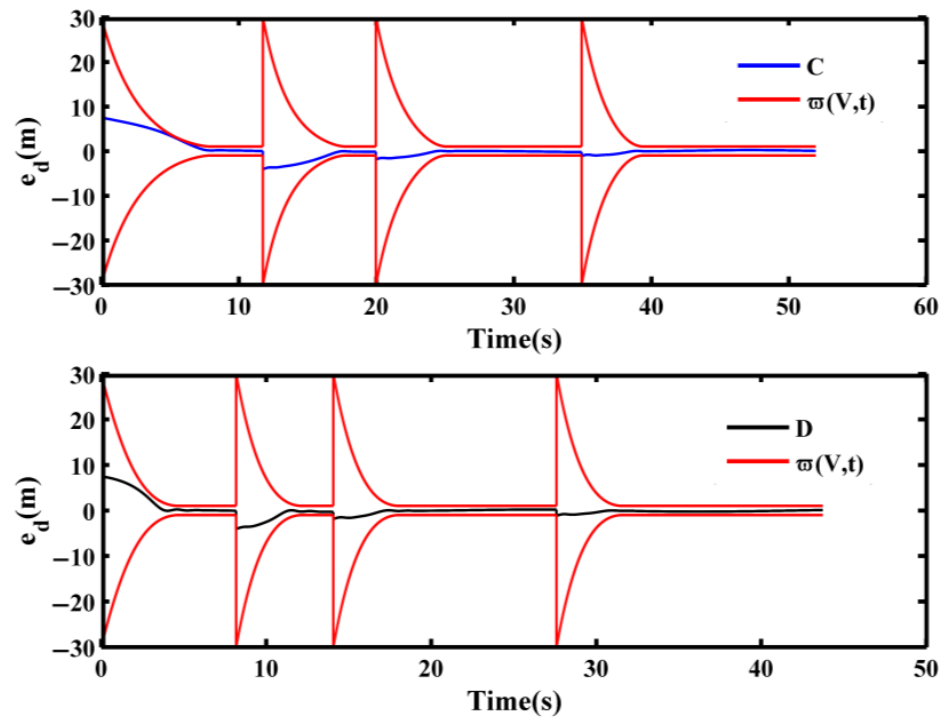


Figure 12. Curves of tracking error changing with time.

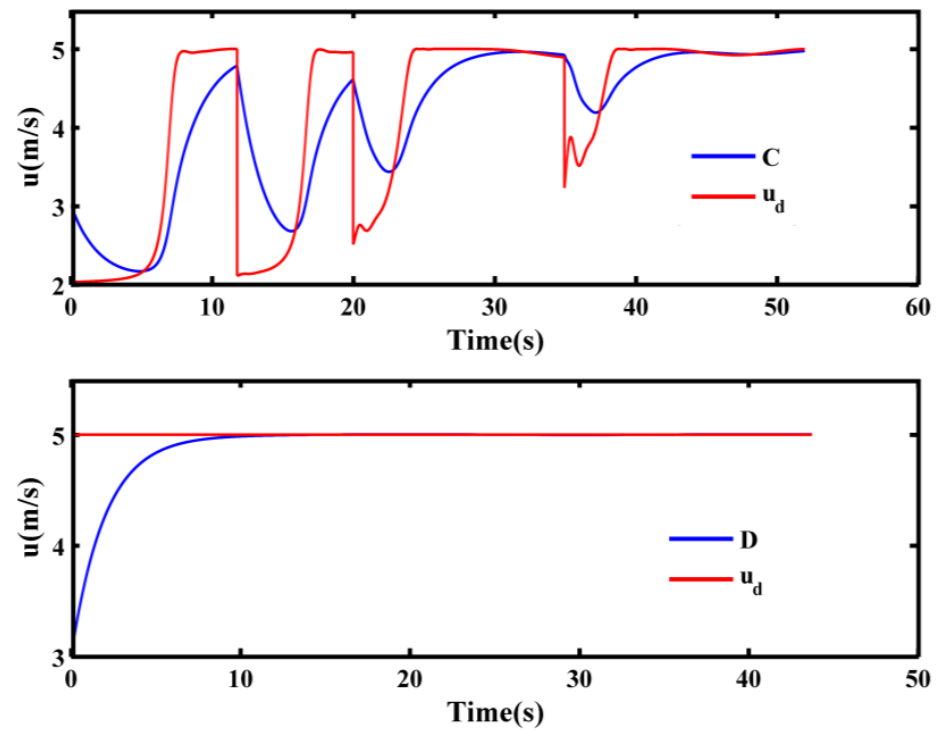


Figure 13. Curves of USV velocity tracking.

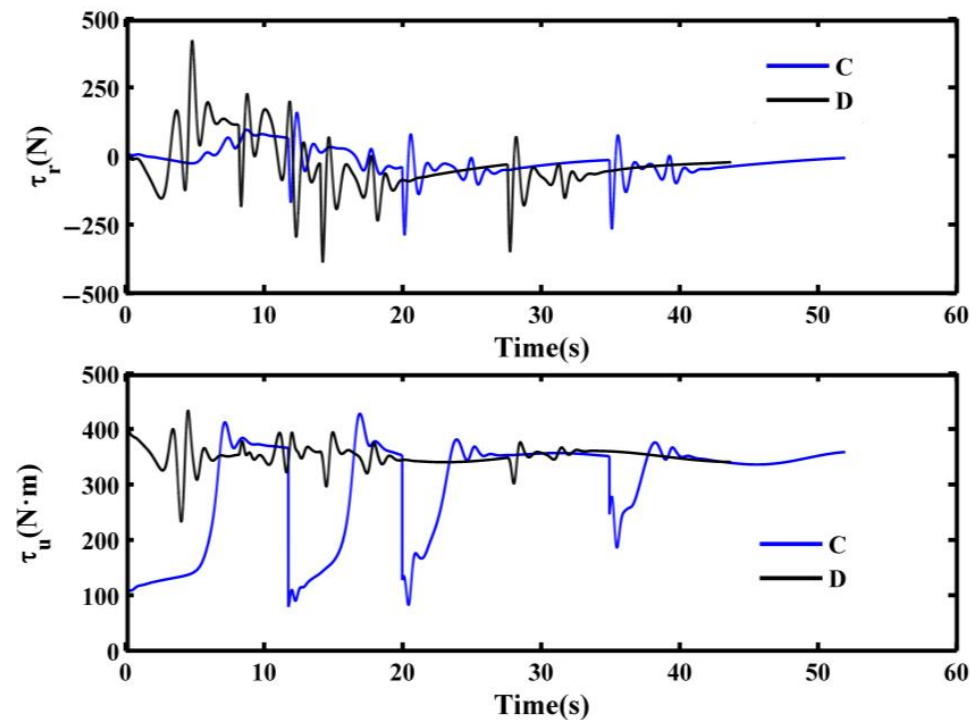


Figure 14. Curves of USV control input.

7. Conclusions

To solve the control problem of path-following and obstacle avoidance of USVs, a guidance and control scheme with finite-distance convergence has been proposed in this paper. The effectiveness of the scheme is proven by theoretical and simulation verification.

1. The designed performance function was used to constrain the path-following error in the finite-distance convergence guidance and control law. Theoretical analysis and simulation experiments demonstrated that the lateral error could converge to a steady-state value within a limited distance, maintaining stability. Throughout path-tracking, the USV successfully avoided obstacles and ensured navigation safety.
2. The designed adaptive velocity command could be adaptively adjusted according to the size of the path-following error. Comparative simulations reveal that when the error increases, the velocity decreases with its command. This approach effectively mitigates heading-actuator saturation to a certain extent, with almost negligible impact on the finite-distance convergence performance of the lateral error. Consequently, the USV retains its proficiency in path-following and obstacle avoidance.

The focus of this study on path-following and obstacle-avoidance control issues for USVs primarily centers on static obstacles, with less consideration given to input-saturation problems. Further research will be carried out on the obstacle-avoidance problem of dynamic obstacles and the limitation of actuators in the future.

Author Contributions: Conceptualization, J.W.; methodology, J.W. and J.Z.; software, J.W. and J.Z.; validation, Z.L.; formal analysis, J.W.; investigation, J.W. and B.S.; resources, J.W. and J.Q.; data curation, J.W.; writing—original draft preparation, J.W. and Y.Z.; writing—review and editing, J.W.; visualization, J.W.; supervision, J.W.; project administration, J.W.; funding acquisition, J.W. All authors have read and agreed to the published version of the manuscript.

Funding: This research received no external funding.

Institutional Review Board Statement: Not applicable.

Informed Consent Statement: Not applicable.

Data Availability Statement: The data that support the findings of this study are available within the article.

Acknowledgments: The authors of this paper would like to express their sincere gratitude to the editors and reviewers for their hard work.

Conflicts of Interest: The authors declare no conflict of interest.

References

1. Fossen, T.I.; Pettersen, K.Y. On uniform semiglobal exponential stability (USGES) of proportional line-of-sight guidance laws. *Automatica* **2014**, *50*, 2912–2917. [[CrossRef](#)]
2. Fossen, T.I.; Breivik, M.; Skjetne, R. Line-of-Sight Path Following of Underactuated Marine Craft. *IFAC Proc. Vol.* **2003**, *36*, 211–216. [[CrossRef](#)]
3. Børhaug, E.; Pavlov, A.; Pettersen, K.Y. Integral LOS Control for Path Following of Underactuated Marine Surface Vessels in the Presence of Constant Ocean Currents. In Proceedings of the 2008 47th IEEE Conference on Decision and Control, Cancun, Mexico, 9–11 December 2008; pp. 4984–4991.
4. Zhu, H.; Yu, H.M.; Guo, C. Finite time PAILOS based path following control of underactuated marine surface vessel with input saturation. *ISA Trans.* **2023**, *135*, 66–77. [[CrossRef](#)] [[PubMed](#)]
5. Hu, C.; Wang, R.R.; Yan, F.J.; Chen, N. Robust Composite Nonlinear Feedback Path-Following Control for Underactuated Surface Vessels with Desired-Heading Amendment. *IEEE Trans. Ind. Electron.* **2016**, *63*, 6386–6394. [[CrossRef](#)]
6. Zhao, Y.J.; Qi, X.; Incecik, A.; Ma, Y.; Li, Z. Broken lines path following algorithm for a water-jet propulsion USV with disturbance uncertainties. *Ocean Eng.* **2020**, *201*, 107118. [[CrossRef](#)]
7. Liu, Z.L.; Li, G.S.; Zhang, J.; Zheng, L. Path following for underactuated surface vessels with disturbance compensating predictive control. *Int. J. Adv. Robot. Syst.* **2020**, *17*, 1729881420920039. [[CrossRef](#)]
8. Liu, Z.Q. Improved ELOS based path following control for underactuated surface vessels with roll constraint. *Ocean Eng.* **2022**, *245*, 110348. [[CrossRef](#)]
9. Xia, G.Q.; Wang, X.W.; Zhao, B.; Han, Z.; Zheng, L. Adaptive Neural Path Following Control of Underactuated Surface Vessels with Input Saturation. *IEEE Access* **2020**, *8*, 82540–92529. [[CrossRef](#)]
10. Xia, G.Q.; Wang, X.W.; Zhao, B.; Han, Z.; Ren, Z. ESHLOS guidance for neuro-adaptive path following control of underactuated surface vessels. *Ocean Eng.* **2022**, *266*, 112894. [[CrossRef](#)]
11. Qin, H.D.; Li, C.P.; Sun, Y.C. Adaptive trajectory tracking algorithm of unmanned surface vessel based on anti-windup compensator with full-state constraints. *Ocean Eng.* **2020**, *200*, 106906. [[CrossRef](#)]
12. Zhang, L.; Zheng, Y.X.; Huang, B. Finite-time trajectory tracking control for under-actuated unmanned surface vessels with saturation constraint. *Ocean Eng.* **2022**, *249*, 110745. [[CrossRef](#)]
13. Qin, H.D.; Chen, X.Y.; Sun, Y.C. Adaptive state-constrained trajectory tracking control of unmanned surface vessel with actuator saturation based on RBFNN and tan-type barrier Lyapunov function. *Ocean Eng.* **2022**, *253*, 110966. [[CrossRef](#)]
14. Qin, H.D.; Li, C.P.; Sun, Y.C. Finite-time trajectory tracking control of unmanned surface vessel with error constraints and input saturations. *J. Frankl. Inst.* **2019**, *357*, 11472–11495. [[CrossRef](#)]
15. Fan, Y.S.; Qiu, B.B.; Liu, L.; Yang, Y. Global fixed-time trajectory tracking control of underactuated USV based on fixed-time extended state observer. *ISA Trans.* **2023**, *132*, 267–277. [[CrossRef](#)] [[PubMed](#)]
16. Wang, S.D.; Sun, M.W.; Xu, Y.H. Predictor-Based Fixed-Time LOS Path Following Control of Underactuated USV With Unknown Disturbance. *IEEE Trans. Intell. Veh.* **2023**, *8*, 2088–2096. [[CrossRef](#)]
17. Chen, L.P.; Cui, R.X.; Yang, C.G.; Yan, W. Adaptive Neural Network Control of Underactuated Surface Vessels with Guaranteed Transient Performance: Theory and Experimental Results. *IEEE Trans. Ind. Electron.* **2020**, *67*, 4024–4035. [[CrossRef](#)]
18. Zhao, Y.J.; Ma, Y.; Hu, S.L. USV Formation and Path-Following Control via Deep Reinforcement Learning With Random Braking. *IEEE Trans. Neural Netw. Learn. Syst.* **2021**, *32*, 5468–5478. [[CrossRef](#)]
19. Zhong, W.B.; Li, H.D.; Meng, Y.Z.; Yang, X.; Feng, Y.; Ye, H.; Liu, W. USV path following controller based on DDPG with composite state-space and dynamic reward function. *Ocean Eng.* **2022**, *266*, 112449. [[CrossRef](#)]
20. Ghommam, J.; Iftekhar, L.; Saad, M. Adaptive Finite-time Path-following Control of Under actuated Surface Vehicle with Collision Avoidance. *J. Dyn. Syst. Meas. Control.* **2019**, *141*, 121008. [[CrossRef](#)]
21. Liu, Z.L.; Song, S.M.; Yuan, S.Z.; Ma, Y.; Yao, Z. ALOS-Based USV Path-Following Control with Obstacle Avoidance Strategy. *J. Mar. Sci. Eng.* **2022**, *10*, 1203. [[CrossRef](#)]
22. Zhang, G.Q.; Han, J.; Zhang, W.D. Finite-time adaptive event-triggered control for USV with COLREGS-compliant collision avoidance mechanism. *Ocean Eng.* **2023**, *285*, 115357. [[CrossRef](#)]
23. Alejandro, G.G.; Ivana, C.G.; Rodolfo, C.U. Path-following and LiDAR-based obstacle avoidance via NMPC for an autonomous surface vehicle. *Ocean Eng.* **2022**, *266*, 112900.
24. Sanchez, I.; D’Jorge, A.; Raffo, G.V.; González, A.H.; Ferramosca, A. Nonlinear Model Predictive Path Following Controller with Obstacle Avoidance. *J. Intell. Robot. Syst.* **2021**, *102*, 1–18. [[CrossRef](#)]
25. Xie, W.J.; Ma, B.L. Robust global uniform asymptotic stabilization of underactuated surface vessels with unknown model parameters. *Int. J. Robust Nonlinear Control.* **2015**, *25*, 1037–1050. [[CrossRef](#)]

26. Wang, B.; Nersesov, S.G.; Ashrafiuon, H. Robust Formation Control and Obstacle Avoidance for Heterogeneous Underactuated Surface Vessel Networks. *IEEE Trans. Control. Netw. Syst.* **2022**, *9*, 125–137. [[CrossRef](#)]
27. Yan, X.; Jiang, D.P.; Miao, R.L.; Li, Y. Formation Control and Obstacle Avoidance Algorithm of a Multi-USV System Based on Virtual Structure and Artificial Potential Field. *J. Mar. Sci. Eng.* **2021**, *9*, 161. [[CrossRef](#)]
28. Manuel, M.; Simone, F. Design and Simulation of a Neuroevolutionary Controller for a Quadcopter Drone. *Aerospace* **2023**, *10*, 418.
29. Farrell, J.A.; Polycarpou, M.; Sharma, M.; Dong, W. Command Filtered Backstepping. *IEEE Trans. Autom. Control.* **2009**, *54*, 1391–1395. [[CrossRef](#)]
30. Bu, X.W.; Wu, X.Y.; Chen, Y.X.; Bai, R.Y. Design of a Class of New Nonlinear Disturbance Observers based on Tracking Differentiators for Uncertain Dynamic Systems. *Int. J. Control. Autom. Syst.* **2015**, *13*, 595–602. [[CrossRef](#)]
31. Bchlioulis, C.P.; Rovithakis, G.A. Prescribed performance adaptive control of SISO feedback linearizable systems with disturbances. In Proceedings of the 2008 16th Mediterranean Conference on Control and Automation, Ajaccio, France, 25–27 June 2008; pp. 1035–1040.
32. Bu, X.W.; Xiao, Y.; Wang, K. A prescribed performance control approach guaranteeing small overshoot for air-breathing hypersonic vehicles via neural approximation. *Aerosp. Sci. Technol.* **2017**, *71*, 485–498. [[CrossRef](#)]

Disclaimer/Publisher’s Note: The statements, opinions and data contained in all publications are solely those of the individual author(s) and contributor(s) and not of MDPI and/or the editor(s). MDPI and/or the editor(s) disclaim responsibility for any injury to people or property resulting from any ideas, methods, instructions or products referred to in the content.